Mass-producible High Performance NiNx Electro-Catalyst Prepared via Surface Immobilization

Qiankun Hou
Cent S University
Kang Liu
Central South University
Yuchang Huang
Cent S University
Walid AL MAKSOUD
King Abdullah University of Science and Technology
Pengfei Yang
Cent S University
De Ding
Shaanxi Electric Power Research Institute
Nan Yang
Cent S University
Tianyong Luo
University of Electronic Science and Technology of China
Yongpeng Lei
Central South University https://orcid.org/0000-0002-8061-4808
Yi Zhang
Central South University https://orcid.org/0000-0002-8452-9694
Li Rong Zheng
Chinese Academy of Sciences
Min Liu
Central South University https://orcid.org/0000-0002-9007-4817
Bin Lin
School of Materials and Energy, University of Electronic Science and Technology of China
Yin Chen (chenyin@iccas.ac.cn)
Cent S University
JEAN BASSET
King Abdullah University of Science and Technology https://orcid.org/0000-0003-3166-8882

Article

Keywords:

Posted Date: February 15th, 2022

DOI: https://doi.org/10.21203/rs.3.rs-990428/v1

Abstract

Nonprecious-metal catalysts with atomically dispersed active sites demonstrated high activity and selectivity in a series of catalysis reactions, the rational design and massive synthesis of such catalysts are of great interest but remains a huge challenge. Current approaches often require harsh conditions and tedious procedures. Here, we demonstrated a facile and scalable preparation strategy by anchoring pre-organized NiNx site on the surface of a layered Co-methylimidazole coordination compound. In two simple steps, single-site Ni electro-catalyst can be synthesized up to kilogram-scale with a yield of 75% under mild conditions. This catalyst exhibits excellent catalysis performances in both oxygen evolution and reduction reactions. Besides, it has tunable catalysis activity, high catalysis reproducibility and stability. The atomically dispersed NiNx sites are tolerate with high Ni concentration, indicating that the random reactions or metal nanoparticle formation generally observed at high temperature were avoided. This strategy presents a practical and green method for the industrial manufacture of nonprecious-metal single-site catalysts with predictable structure.

Full Text

Heterogeneous catalysts with atomically dispersed active-sites represent the most active and attractive area in catalysis, owing to their high activity and selectivity in variety of catalytic reactions.[1-4] As we know, early transition-metal can form strong M-O bond, which can be immobilized on the support to produce single-sited catalysts. Contrastively, it's challenging to immobilize noble metals or first-row late transition metals on substrate surfaces, where they tend to aggregate and form nanoparticles. During the past decade, by trapping the metal atom with the vacancy defects of the support materials (such as nitrogen-rich carbon or metal oxides),[5,6] single atom catalysts (SAC) have emerged as the quasi-molecular heterogenous catalyst, and different strategies have been developed for both nonprecious-metal and noble metal SAC. [7-10]

Currently, SACs usually prepared under very high temperature (800-1100 ^{o}C). Random reactions are inevitable under classical condition; the metal atoms tend to aggregate and form metal nanoparticles. As a result, it is difficult to increase the content of active metal species in the catalyst. Meanwhile, the as-prepared SACs are inclined to a spontaneously generated thermodynamically stable structure instead of a predictable or tunable "molecular like" structure. Although outstanding performance and stability have been observed in thermal-catalysis and electro-catalysis, the tedious and costly synthetic process, low yield and active metal content still exist as the main obstacles for the large-scale application of SACs.[11] Thus, the development of a scalable and straightforward synthesis strategy for atomically dispersed non-precious catalyst under mild conditions is urgent for industrial application.

Porphyrin-like MN_xC_x site is regarded as a promising archetypical catalysis active species.[12-21] Several interesting and pioneering examples confirmed that pre-organized MN_x site is quite active in catalysis reaction. For example, Porphyrin type CoN_4 has high electro-catalysis activity when located on graphene

without pyrolysis.[22] Porphyrin FeN_4 site can be implanted into graphene to produce active catalyst by ball-milling at room temperature.[13] Well-dispersed surface $Fe(phen)_x$ or Fe-Bipy can be converted into catalysis active FeN_4C_x site at relatively low temperature (500 - 600 ^oC).[15,23] It have been concluded that the active MN_x site can be produced not only by trapping metal atom with vacancy defects at very high temperature, but also by anchoring the pre-organized MN_x species via organic reactions under very mild conditions. Starting from the precursor with pre-existing MN_x structure, Porphyrin-like MN_xC_x site prospectively can be immobilized on the support surface,[24] resulting in a predictive and scalable preparation approach for the MN_x type catalyst, which is similar to the surface organometallic chemistry (SOMC) strategy in some extent.[25-29]

Herein, by anchoring NiN_x precursor (bis(ethylenediamine)nickel(II) chloride) on the surface of a layered metal-organic coordination compound, we demonstrated a facile strategy for large-scale production of single-sited NiN_x with excellent electro-catalysis performance. This single-sited NiN_x catalyst can be easily and rationally synthesized within two simply steps. After dispersing on the substrate surface, NiN_x precursor were effectively immobilized after treatment under 350 ^oC in ordinary muffle furnace, as shown in the schematic diagram Fig. 1A. The amino-sugar core of the intercalated surfactant dehydrated at high temperature to generate C=O group, which condensed with the precursor to from NiN_xC_x site *in situ* (*via* Maillard reaction). Random reactions were avoided at the low reaction temperature, the resulting catalyst has fully tuneable metal concentration, catalysis activity, high reproducibility and stability. It exhibit excellent performance in both oxygen reduction/evolution reaction (the calculated ΔE is up to 0.69 V and is identical to previous reported SAC Ni-NHGF[6]). In addition, this catalyst can be easily prepared in tens of grams in one batch from cheap starting materials with simple equipment. It presents a commercially viable way for the large-scale production of NiN_x catalyst with tuneable electrocatalysis performance.[16,24,30-36]

The multi-layered metal coordination compound (MLM) was prepared from $Co(NO_3)_2$ and imidazole in the emulsion of water/dichloromethane with SAAS-C_{12} as surfactant.[37-39] The multi-layered structure of MLM was confirmed by the transmission electron microscopy (TEM) images (Fig. S1, S2). MLM can be exfoliated into ultra-thin nanosheets in dichloromethane, obvious Tyndall effect can be observed (Fig. 2A). The scanned electron microscopy (SEM) images reveal that the nanosheets are quite flat with large lateral size. Powder X-ray diffraction (XRD) patterns show that MLM samples have a main diffraction peak around 14^o, which is consist with the raw Co-imidazole coordination compound (Fig. S3).[39,40] The PXRD patterns of MLM samples remained nearly the same with different additive amount of NiN_x precursor (bis(ethylenediamine)nickel(II) chloride): MLM1 (Ni/Co=1:30), MLM2 (Ni/Co =1:15), MLM3 (Ni/Co =1:7.5), MLM4 (Ni/Co =1:2).

For MLM2, inductively coupled plasma optical emission spectrometer (ICP-OES) identified a Ni/Co atomic ratio around 1:16 (10.9 wt% for Co, 0.7 wt% for Ni), but X-ray photoelectron spectroscopy (XPS, Table S1, Fig. S4) found a Ni/Co ratio as 1:6 for the near-surface. Meanwhile, Energy Dispersive X-ray Spectroscopy

(EDS) images revealed a homogeneous Ni element signal intensity (Figure 2C). It can be concluded that the NiN_x precursor didn't interfere in the formation of MLM and most possibly dispersed homogenously between the layers in the emulsion synthesis (Fig 1A, detailed information see SI).

To immobilize the NiN_x site on the surface, MLM samples were put into muffle furnace and treated under the target temperature for 2 hours in a covered alumina crucible with a ramping rate as 2 °C/min. Popcorn-like product was obtained for MLM2 at 350 °C, which was labeled as MLM2-350 (Figure 1B, S5). SAAS-C_{12} has an amino sugar core, which dehydrates at high temperature and plays the role as a binder to anchor the NiN_x site. ICP-OES results found a Ni/Co atomic ratio around 1:17 for MLM2-350 (27.0 wt% for Co, 1.6 wt% for Ni), and XPS data revealed the value to be 1:10 (Table S1, Fig. S6). The total yield for MLM2-350 in two steps is around 75% based on the quantity of $Co(NO_3)_2 \cdot 6H_2O$ used. No diffraction peak can be observed in the PXRD pattern of MLM2-350 (Fig. 2D, S7), suggesting the atomical dispersion of the metal species and the absence of metallic or metal oxide crystallites. Even higher pyrolysis temperatures led to the decomposition of the organic components and the formation of Co_3O_4, strong characteristic diffraction peaks of Co_3O_4 were observed for MLM2-550.[41] TG analysis found that the weight loss of MLM2 before 300 °C mainly can be attributed to the loss of water and decomposition of SAAS-C12 (Fig. S8), as $Co(Im)_2$ coordination polymer is stable up to 400 °C.[42] Reducing gas produced in the process expanded the sample and protected it from oxidation in the alumina crucible. IR spectra confirmed the formation of C=O groups in the thermal treatment of MLM, which reacted with the precursor to form NiN_xC_x site in the following reactions (Fig. S9, S10). Raman spectra identified the as-prepared MLM2-350 as a defect-rich carbon material (Fig. 2E).

XPS was used to assess the composition and speciation of C, N, Ni and Co species in different MLM samples (Fig. 3, S11, S12). The Co2p binding energy signal at 781.5 eV remained the same for different MLM-350 samples, which further confirmed the role of MLM as a support material. The Ni2p binding energy signal around 855.0 eV increased reasonably with the loading amount of precursor. Characteristic C1s XPS peak around 288.0 eV appeared after the thermal treatment, which can be attributed to the C=O group formed due to dehydration. Its intensity decreased in inverse proportion to the NiN_x precursor loading amount. Obviously, the C=O group generated *in situ* was consumed in the reaction with precursor, which was further identified by the IR spectra (Fig. 2F), a simultaneously decrease of oxygen composition in MLM also was observed by XPS (Table S1). Meanwhile, the N1s peak around 400.2 eV increased proportionately (Table S2), supporting the reaction of NiN_x moiety with C=O group.

As compared to MLM2, the C1s and N1s binding energy peaks of MLM2-350 decreased 1-2 eV to 284.5 eV and 398.7 eV respectively (Fig. S13). Meanwhile, the C=N and C=C components significantly increased. That can be attributed to the formation of big conjugated heterocycles in the carbonization process. Possible reaction mechanism can be concluded, which is similar to the Maillard reaction:[43] the amino-sugar surfactant dehydrated above 170 °C to generate C=O species, which reacted with the NH_2 group of precursor molecule in the nearby to form imine type NiN_x; as a result, the NiN_x site was

immobilized on the layer surface (Scheme S1). Under 350 ^{o}C, Ni-N or C-C bonds still are stable, but carbon-heteroatom bonds become active, rearrangement and aromatization reactions took place, catalyst,[44-46] leading to the formation of atomically dispersed active NiN_xC_x sites, as shown in Fig 1C.

TEM images indicated that the layered structure of MLM disappeared after thermal treatment, but no nanoparticle can be found (Fig. 4A, S14, S15). Obviously, the layers were cross-linked during the carbonization process. High Angle Annular Dark Field scanning TEM (HAADF-STEM) and corresponding element mapping (Fig. 4B, S16) images revealed a uniform distribution of C, N, Ni and Co elements throughout the MLM2-350 samples. The atomic structure of metal species in MLM2-350 was further imaged by aberration corrected HAADF-STEM, and evenly dispersed bright dots can be clearly observed from this N-rich carbon material (Figure 4C, S17).

The chemical and atomic structure of MLM-350 samples were further analyzed by X-ray absorption spectroscopy (XAS).[14,19,35,47] Ni K-edge X-ray absorption near-edge structure (XANES) spectra of different MLM samples present quite similar near-edge absorption energy, which is close to that of standard NiPc sample and far away from metal oxides or metal foils, also fits the previous reports of NiN_x SAC (Fig. 4D, S18).[6] The corresponding Fourier transformed extended X-ray absorption fine structure spectra (FT-EXAFS) of MLM-350 in R space show only one dominant peak at 1.88 Å, which can be assigned to the Ni-N coordination at the first shell (Fig. 4E, 4F). No intensity maximum belonging to Ni-Ni/Ni-Co contribution can be observed, comparing with the wavelet transforms (WT) plots of MLM-350 samples (Fig. S19), the possibility of any Ni or Ni/Co clusters or nanoparticles can be excluded. The coordination structures around Ni atoms were clarified by fitting the FT-EXAFS data. The optimized coordination number of Ni-N for MLM2-350 is around 3.2, implying that each nickel atom is likely coordinated with three to four nitrogen atoms (Table S3). Different MLM-350 samples gave very close Co K-edge XANES and EXAFS spectra (Fig. S20-S23), which further confirmed the role of MLM only as a substrate, which didn't influence by the addition of NiN_x precursor. Comparison of the first derivative XANES with references indicates that the valence states for Co is approximately +2, each Co atom is likely coordinated with four nitrogen/oxygen atoms (Table S4). Meanwhile, No Co-Co or Ni-Co path around 2.2 Å can be observed, indicating that the Co atoms exist in single atom state even with extremely high concentration.

Based on EXAFS-WT, EXAFS-FT and XANES analyses, it can be concluded that the NiN_x moieties were atomically dispersed as expected, which was immobilized on the surface *via* organic reaction at relatively mild conditions. Since many previous researches have investigated the electro-catalysis activity of MN_x site in oxygen evolution reaction (OER) and oxygen reduction reactions (ORR), by comprehensive comparison of the catalysis performance of MLM with the reported catalysts,[48-51] we can further verify the validity of our synthesis strategy.

Catalytic performance of MLM samples in OER and ORR were evaluated systematically in 1 M KOH (Fig. 5). MLM2-350 has the best catalytic activity in both OER and ORR among all these samples for a moderate NiN_x concentration and immobilization reaction temperature.

Fig. 5A shows the OER test results of MLM2 after treatment at increasing temperatures from RT to 550 ^{o}C. The newly prepared MLM2 has an overpotential of 376 mV (at 10 mA/cm^{-2} current density) in OER (Fig. S24). After thermal treatment under 350 ^{o}C, the observed overpotential in OER decreased to 340 mV with a lower Tafel slope as 59 mV dec^{-1} (Fig. 5C). The electrochemical impedance spectroscopy also revealed that MLM2-350 has the lowest charge transfer resistance (Fig. S25). The enhanced catalysis performance can be attributed to the formation of large conjugation structure and immobilized NiN_xC_x site in the carbonization reaction (including dehydrogenation, rearrangement and aromatization reactions). 350 ^{o}C is an ideal choice for this process, as the reaction process is not favored at low temperature, and too high a temperature will destroy the organic component and catalysis activity (Fig. 5B). Long time thermal treatment also is disadvantageous for the structure stability and catalysis activity (Fig. S26).

The OER performance of MLM-350 is significantly influenced by the loading amount of NiN_4 precursor, which was enhanced at first (Fig. S27), but even higher NiN_x loading leads to a poor catalysis performance. Chronopotentiometric curve show that MLM2-350 possesses outstanding operation activity and durability in OER reaction, as its OER overpotential even slightly decreased to 330 mv after 10 h continuous test in 1 M KOH solution (Fig. S28).

The ORR activity of different MLM samples were further investigated *via* linear scan voltammogram (LSV) and Cyclic voltammetry (CV) in 1.0 M KOH (saturated by O_2). MLM2-350 also exhibited a distinguished onset potential (E_{onset} = 1.06 V) and half-wave potential ($E_{1/2}$ = 0.87 V, 0.07 V higher than Pt/C). The measured Tafel slope value for MLM2-350 in ORR is only 51 mV dec^{-1}, indicating a favored ORR kinetic process (Fig. 4D, S29, S30).

The calculated electron transfer number (n) of MLM2-350 in ORR is 3.98 (Fig. S31), which is close to the theoretical value (4.0). The kinetic current density of MLM2-350 demonstrated an incredibly high JK as 45.9 mA cm^{-2} (Fig. S32), which was 27 times higher than that of Pt/C (1.7 mA cm^{-2}). MLM2-350 has a high tolerance to methanol in ORR, no significant performance decay was found after continuous cycling CVs of 5000 cycles with RDE (Fig. S33). These results identified the outstanding catalysis stability of MLM2-350 in ORR. CV curves further confirmed the outstanding oxygen electro-catalysis performance of MLM2-350, which own the best electrochemical double-layer capacitance among these samples as 114.5 mF/cm^2 (Fig. S34, S35). The influence of pyrolysis temperature and time, precursor loading amount to the ORR performance of MLM2-350 keeps pace with what observed in OER (Fig. S32, S36, S37).

Compare to Ni-NHGFs, a well-defined NiN_x SAC in previous report,[6] MLM2-350 exhibited an identical catalysis performance, such as polarization curve, Tafel curve and calculated ΔE (ΔE = $E_{OER} - E_{1/2ORR}$, Fig. 5E), indicating they have very similar active NiN_x site. Although with an Ni content as 1.5 wt% (0.05% for Ni-NHGFs), the quite low BET surface area (27 m^2/g) of MLM2-350 is disadvantageous for the improvement of electro-catalysis performance. The calculated ΔE for MLM2-350 is around 0.70 V, which is the best among the NiN_x type electrocatalysts up to our knowledge (Table S5). MLM2-350 prepared in

different batches have consistent electro-catalysis performance in OER and ORR, which supports the high reproducibility of the NiN_x sites (Fig. S38).

In heterogeneous catalysis, the catalysis efficiency generally increases with the concentration of exposed catalytic active sites, but too high concentration causes the aggregation of active sites and destroys the catalysis efficiency and selectivity in turn. From the polarization and Tafel curves of MLM1-350, MLM2-350, MLM3-350, it can be concluded that they share similar active species, but different active site concentration resulted in the different electro-catalysis current density. Very high precursor loading and different thermal treatment temperatures led to different surface Ni species, which have lower catalysis activity and different polarization curves.

In summary, we have demonstrated an attractive strategy for the synthesis of high performance single-sited NiN_x electrocatalyst. Instead of trapping the Ni atom into nitrogen-rich porous carbon, the success of this strategy lies on anchoring the NiN_x moiety on the support surface *via* organic reactions *in situ* to produce active NiN_xC_x site. In hence, much low reaction temperature is needed. The as-prepared NiN_x catalyst has tunable catalytic performance and high design flexibility. It can be synthesized in large batch easily with unprecedent yield and high metal content from cheap starting material. The as-prepared MLM2-350 also exhibited excellent electro-catalysis performance, with an initial overpotential of 340 mV at 10 mA cm^{-2} for OER and a half-potential ($E_{1/2}$) of 0.87 V for ORR, presenting a commercially viable high-performance electro-catalyst. This study has developed a practical and green method for the industrial manufacture of atomically dispersed nonprecious-metal catalysts with predictable structure.

Declarations

AUTHOR INFORMATION

Corresponding Author

Prof. Yin Chen E-mail: chenyin@iccas.ac.cn

Prof. Bin Lin E-mail: bin@uestc.edu.cn

Prof. Min Liu E-mail: minliu@csu.edu.cn

Prof. Lirong Zheng E-mail: zhenglr@ihep.ac.cn

Author contributions: Q. H. developed the material, conducted part of material characterization and electro-chemical analysis; K. L. and L. Z. performed the synchrotron radiation X-ray analysis and DFT calculation; Y. H. conducted the large-scale preparation and part of material characterization; W. A.-M. performed the TEM and aberration-corrected HAADF-STEM; P. Y. performed the nanosheets exfoliation and structure characterization; N. Y., D. D., T. L., Y. L., Y. Z. took part in the electro-chemical analysis and

data analysis; Y. C. supervised the research; Y.C., B. J.-M., B. L., M. L. designed the experiments of this projects and wrote the manuscript. All authors discussed, commented on and revised the manuscript.

Acknowledgements: We thank Prof. Enrico Traversa for helpful discussion, Prof. Jianglan Shui, Xiaohui Gao for support in synchrotron radiation X-ray analysis. We acknowledge financial support from Central South University, NSF of China and KAUST. The authors acknowledge the resources and facilities provided by Central South University, BSRF, KAUST Core Labs and University of Electronic Science and Technology of China. B. L. thanks the financial support from the University of Electronic Science and Technology of China and the Thousand Talents Plan of Sichuan Province.

Competing interests

The authors declare no competing financial interests.

Additional information

Supplementary information is available for this paper.

References

1. Yang, X.-F., Wang, A., Qiao, B., Li, J., Liu, J., and Zhang, T. (2013). Single-Atom Catalysts: A New Frontier in Heterogeneous Catalysis. Accounts of Chemical Research *46*, 1740-1748. 10.1021/ar300361m.

2. Coperet, C., Chabanas, M., Saint-Arroman, R.P., and Basset, J.M. (2003). Homogeneous and heterogeneous catalysis: Bridging the gap through surface organometallic chemistry. Angewandte Chemie-International Edition *42*, 156-181. 10.1002/anie.200390072.

3. Pelletier, J.D.A., and Basset, J.-M. (2016). Catalysis by Design: Well-Defined Single-Site Heterogeneous Catalysts. Accounts of Chemical Research *49*, 664-677. 10.1021/acs.accounts.5b00518.

4. Wang, A., Li, J., and Zhang, T. (2018). Heterogeneous single-atom catalysis. Nature Reviews Chemistry *2*, 65-81. 10.1038/s41570-018-0010-1.

5. Qiao, B., Wang, A., Yang, X., Allard, L.F., Jiang, Z., Cui, Y., Liu, J., Li, J., and Zhang, T. (2011). Single-atom catalysis of CO oxidation using Pt-1/FeOx. Nature Chemistry *3*, 634-641. 10.1038/nchem.1095.

6. Fei, H.L., Dong, J.C., Feng, Y.X., Allen, C.S., Wan, C.Z., Volosskiy, B., Li, M.F., Zhao, Z.P., Wang, Y.L., Sun, H.T., et al. (2018). General synthesis and definitive structural identification of MN4C4 single-atom catalysts with tunable electrocatalytic activities. Nature Catalysis *1*, 63-72. 10.1038/s41929-017-0008-y.

7. Wu, X., Zhang, H., Zuo, S., Dong, J., Li, Y., Zhang, J., and Han, Y. (2021). Engineering the Coordination Sphere of Isolated Active Sites to Explore the Intrinsic Activity in Single-Atom Catalysts.

Nano-Micro Letters *13*, 136. 10.1007/s40820-021-00668-6.

8. Ji, S., Chen, Y., Wang, X., Zhang, Z., Wang, D., and Li, Y. (2020). Chemical Synthesis of Single Atomic Site Catalysts. Chemical Reviews *120*, 11900-11955. 10.1021/acs.chemrev.9b00818.

9. Guo, W., Wang, Z., Wang, X., and Wu, Y. (2021). General Design Concept for Single-Atom Catalysts toward Heterogeneous Catalysis. Advanced Materials, 2004287. 10.1002/adma.202004287.

10. Kaiser, S.K., Chen, Z., Akl, D.F., Mitchell, S., and Perez-Ramirez, J. (2020). Single-Atom Catalysts across the Periodic Table. Chemical Reviews *120*, 11703-11809. 10.1021/acs.chemrev.0c00576.

11. Xia, C., Qiu, Y., Xia, Y., Zhu, P., King, G., Zhang, X., Wu, Z., Kim, J.Y., Cullen, D.A., Zheng, D., et al. (2021). General synthesis of single-atom catalysts with high metal loading using graphene quantum dots. Nature Chemistry. 10.1038/s41557-021-00734-x.

12. Guo, X., Fang, G., Li, G., Ma, H., Fan, H., Yu, L., Ma, C., Wu, X., Deng, D., Wei, M., et al. (2014). Direct, Nonoxidative Conversion of Methane to Ethylene, Aromatics, and Hydrogen. Science *344*, 616-619. 10.1126/science.1253150.

13. Deng, D., Chen, X., Yu, L., Wu, X., Liu, Q., Liu, Y., Yang, H., Tian, H., Hu, Y., Du, P., et al. (2015). A single iron site confined in a graphene matrix for the catalytic oxidation of benzene at room temperature. Science Advances *1*, e1500462. 10.1126/sciadv.1500462.

14. Yin, P., Yao, T., Wu, Y., Zheng, L., Lin, Y., Liu, W., Ju, H., Zhu, J., Hong, X., Deng, Z., et al. (2016). Single Cobalt Atoms with Precise N-Coordination as Superior Oxygen Reduction Reaction Catalysts. Angewandte Chemie-International Edition *55*, 10800-10805. 10.1002/anie.201604802.

15. Liu, W., Zhang, L., Liu, X., Liu, X., Yang, X., Miao, S., Wang, W., Wang, A., and Zhang, T. (2017). Discriminating Catalytically Active FeNx Species of Atomically Dispersed Fe-N-C Catalyst for Selective Oxidation of the C-H Bond. Journal of the American Chemical Society *139*, 10790-10798. 10.1021/jacs.7b05130.

16. Jiang, K., and Wang, H. (2018). Electrocatalysis over Graphene Defect-Coordinated Transition-Metal Single-Atom Catalysts. Chem *4*, 194-195. 10.1016/j.chempr.2018.01.013.

17. Wei, S., Li, A., Liu, J.-C., Li, Z., Chen, W., Gong, Y., Zhang, Q., Cheong, W.-C., Wang, Y., Zheng, L., et al. (2018). Direct observation of noble metal nanoparticles transforming to thermally stable single atoms. Nature Nanotechnology *13*, 856-+. 10.1038/s41565-018-0197-9.

18. Xu, H., Cheng, D., Cao, D., and Zeng, X.C. (2018). A universal principle for a rational design of single-atom electrocatalysts. Nature Catalysis *1*, 339-348. 10.1038/s41929-018-0063-z.

19. Yang, H.B., Hung, S.-F., Liu, S., Yuan, K., Miao, S., Zhang, L., Huang, X., Wang, H.-Y., Cai, W., Chen, R., et al. (2018). Atomically dispersed Ni(i) as the active site for electrochemical CO2 reduction. Nature

Energy *3*, 140-147. 10.1038/s41560-017-0078-8.

20. Zhao, L., Zhang, Y., Huang, L.-B., Liu, X.-Z., Zhang, Q.-H., He, C., Wu, Z.-Y., Zhang, L.-J., Wu, J., Yang, W., et al. (2019). Cascade anchoring strategy for general mass production of high-loading single-atomic metal-nitrogen catalysts. Nature Communications *10*, 1278. 10.1038/s41467-019-09290-y.

21. Yan, H., Lin, Y., Wu, H., Zhang, W., Sun, Z., Cheng, H., Liu, W., Wang, C., Li, J., Huang, X., et al. (2017). Bottom-up precise synthesis of stable platinum dimers on graphene. Nature Communications *8*, 1070. 10.1038/s41467-017-01259-z.

22. Guo, J., Lin, C.-Y., Xia, Z., and Xiang, Z. (2018). A Pyrolysis-Free Covalent Organic Polymer for Oxygen Reduction. Angewandte Chemie-International Edition *57*, 12567-12572. 10.1002/anie.201808226.

23. Ma, L., Chen, S., Pei, Z., Huang, Y., Liang, G., Mo, F., Yang, Q., Su, J., Gao, Y., Zapien, J.A., and Zhi, C. (2018). Single-Site Active Iron-Based Bifunctional Oxygen Catalyst for a Compressible and Rechargeable Zinc–Air Battery. ACS Nano *12*, 1949-1958. 10.1021/acsnano.7b09064.

24. Sun, J., Lowe, S.E., Zhang, L., Wang, Y., Pang, K., Wang, Y., Zhong, Y., Liu, P., Zhao, K., Tang, Z., and Zhao, H. (2018). Ultrathin Nitrogen-Doped Holey Carbon@Graphene Bifunctional Electrocatalyst for Oxygen Reduction and Evolution Reactions in Alkaline and Acidic Media. Angewandte Chemie-International Edition *57*, 16511-16515. 10.1002/anie.201811573.

25. Basset, J.M., and Ugo, R. (2009). On the Origins and Development of “Surface Organometallic Chemistry”. Modern Surface Organometallic Chemistry, 1-21. 10.1002/9783527627097.ch1

26. Serna, P., and Gates, B.C. (2014). Molecular Metal Catalysts on Supports: Organometallic Chemistry Meets Surface Science. Accounts of Chemical Research *47*, 2612-2620. 10.1021/ar500170k.

27. Samantaray, M.K., D’Elia, V., Pump, E., Falivene, L., Harb, M., Ould Chikh, S., Cavallo, L., and Basset, J.-M. (2020). The Comparison between Single Atom Catalysis and Surface Organometallic Catalysis. Chemical Reviews *120*, 734-813. 10.1021/acs.chemrev.9b00238.

28. Thomas, J.M., Raja, R., and Lewis, D.W. (2005). Single-site heterogeneous catalysts. Angewandte Chemie-International Edition *44*, 6456-6482. 10.1002/anie.200462473.

29. Serna, P., and Gates, B.C. (2011). A Bifunctional Mechanism for Ethene Dimerization: Catalysis by Rhodium Complexes on Zeolite HY in the Absence of Halides. Angewandte Chemie-International Edition *50*, 5528-5531. 10.1002/anie.201008086.

30. Rodenas, T., Beeg, S., Spanos, I., Neugebauer, S., Girgsdies, F., Algara-Siller, G., Schleker, P.P.M., Jakes, P., Pfaender, N., Willinger, M., et al. (2018). 2D Metal Organic Framework-Graphitic Carbon

Nanocomposites as Precursors for High-Performance O-2-Evolution Electrocatalysts. Advanced Energy Materials *8*, 1802404. 10.1002/aenm.201802404.

31. Wang, X.-L., Dong, L.-Z., Qiao, M., Tang, Y.-J., Liu, J., Li, Y., Li, S.-L., Su, J.-X., and Lan, Y.-Q. (2018). Exploring the Performance Improvement of the Oxygen Evolution Reaction in a Stable Bimetal-Organic Framework System. Angewandte Chemie-International Edition *57*, 9660-9664. 10.1002/anie.201803587.

32. Zang, W., Sumboja, A., Ma, Y., Zhang, H., Wu, Y., Wu, S., Wu, H., Liu, Z., Guan, C., Wang, J., and Pennycook, S.J. (2018). Single Co Atoms Anchored in Porous N-Doped Carbon for Efficient Zinc-Air Battery Cathodes. Acs Catalysis *8*, 8961-8969. 10.1021/acscatal.8b02556.

33. Jiang, H., Gu, J., Zheng, X., Liu, M., Qiu, X., Wang, L., Li, W., Chen, Z., Ji, X., and Li, J. (2019). Defect-rich and ultrathin N doped carbon nanosheets as advanced trifunctional metal-free electrocatalysts for the ORR, OER and HER. Energy & Environmental Science *12*, 322-333. 10.1039/c8ee03276a.

34. Lu, Z., Wang, B., Hu, Y., Liu, W., Zhao, Y., Yang, R., Li, Z., Luo, J., Chi, B., Jiang, Z., et al. (2019). An Isolated Zinc-Cobalt Atomic Pair for Highly Active and Durable Oxygen Reduction. Angewandte Chemie-International Edition *58*, 2622-2626. 10.1002/anie.201810175.

35. Yang, Z., Zhao, C., Qu, Y., Zhou, H., Zhou, F., Wang, J., Wu, Y., and Li, Y. (2019). Trifunctional Self-Supporting Cobalt-Embedded Carbon Nanotube Films for ORR, OER, and HER Triggered by Solid Diffusion from Bulk Metal. Advanced Materials *31*, 1808043. 10.1002/adma.201808043.

36. Mistry, H., Varela, A.S., Kuehl, S., Strasser, P., and Cuenya, B.R. (2016). Nanostructured electrocatalysts with tunable activity and selectivity. Nature Reviews Materials *1*, 16009. 10.1038/natrevmats.2016.9.

37. Zhao, M., Huang, Y., Peng, Y., Huang, Z., Ma, Q., and Zhang, H. (2018). Two-dimensional metal-organic framework nanosheets: synthesis and applications. Chem. Soc. Rev. *47*, 6267-6295. 10.1039/c8cs00268a.

38. Junggeburth, S.C., Diehl, L., Werner, S., Duppel, V., Sigle, W., and Lotsch, B.V. (2013). Ultrathin 2D Coordination Polymer Nanosheets by Surfactant-Mediated Synthesis. J. Am. Chem. Soc. *135*, 6157-6164. 10.1021/ja312567v.

39. Zhang, P., Chen, C., Kang, X., Zhang, L., Wu, C., Zhang, J., and Han, B. (2018). In situ synthesis of sub-nanometer metal particles on hierarchically porous metal-organic frameworks via interfacial control for highly efficient catalysis. Chemical Science *9*, 1339-1343. 10.1039/c7sc04269h.

40. Xiao, X., He, C.-T., Zhao, S., Li, J., Lin, W., Yuan, Z., Zhang, Q., Wang, S., Dai, L., and Yu, D. (2017). A general approach to cobalt-based homobimetallic phosphide ultrathin nanosheets for highly efficient oxygen evolution in alkaline media. Energy & Environmental Science *10*, 893-899. 10.1039/c6ee03145e.

41. Li, H.-C., Zhang, Y.-J., Hu, X., Liu, W.-J., Chen, J.-J., and Yu, H.-Q. (2018). Metal-Organic Framework Templated Pd@PdO-Co3O4 Nanocubes as an Efficient Bifunctional Oxygen Electrocatalyst. Advanced Energy Materials *8*, 1702734, 1702734. 10.1002/aenm.201702734.

42. Shi, Q., Chen, Z., Song, Z., Li, J., and Dong, J. (2011). Synthesis of ZIF-8 and ZIF-67 by Steam-Assisted Conversion and an Investigation of Their Tribological Behaviors. Angewandte Chemie-International Edition *50*, 672-675. 10.1002/anie.201004937.

43. Mottram, D.S., Wedzicha, B.L., and Dodson, A.T. (2002). Acrylamide is formed in the Maillard reaction. Nature *419*, 448-449. 10.1038/419448a.

44. Kidena, K., Murata, S., and Nomura, M. (1996). Studies on the Chemical Structural Change during Carbonization Process. Energy & Fuels *10*, 672-678. 10.1021/ef9501096.

45. Wang, T., Zhai, Y., Zhu, Y., Li, C., and Zeng, G. (2018). A review of the hydrothermal carbonization of biomass waste for hydrochar formation: Process conditions, fundamentals, and physicochemical properties. Renewable & Sustainable Energy Reviews *90*, 223-247. 10.1016/j.rser.2018.03.071.

46. Zhao, B., O'Connor, D., Zhang, J., Peng, T., Shen, Z., Tsang, D.C.W., and Hou, D. (2018). Effect of pyrolysis temperature, heating rate, and residence time on rapeseed stem derived biochar. Journal of Cleaner Production *174*, 977-987. 10.1016/j.jclepro.2017.11.013.

47. Wang, J., Huang, Z., Liu, W., Chang, C., Tang, H., Li, Z., Chen, W., Jia, C., Yao, T., Wei, S., et al. (2017). Design of N-Coordinated Dual-Metal Sites: A Stable and Active Pt-Free Catalyst for Acidic Oxygen Reduction Reaction. Journal of the American Chemical Society *139*, 17281-17284. 10.1021/jacs.7b10385.

48. Lu, B., Liu, Q., and Chen, S. (2020). Electrocatalysis of Single-Atom Sites: Impacts of Atomic Coordination. Acs Catalysis *10*, 7584-7618. 10.1021/acscatal.0c01950.

49. Yang, J., Li, W., Wang, D., and Li, Y. (2020). Electronic Metal-Support Interaction of Single-Atom Catalysts and Applications in Electrocatalysis. Advanced Materials *32*, 2003300. 10.1002/adma.202003300.

50. Zhang, Q., and Guan, J. (2020). Single-Atom Catalysts for Electrocatalytic Applications. Advanced Functional Materials *30*, 2000768. 10.1002/adfm.202000768.

51. Li, S., Chen, B., Wang, Y., Ye, M.-Y., van Aken, P.A., Cheng, C., and Thomas, A. (2021). Oxygen-evolving catalytic atoms on metal carbides. Nature Materials. 10.1038/s41563-021-01006-2.

Figures

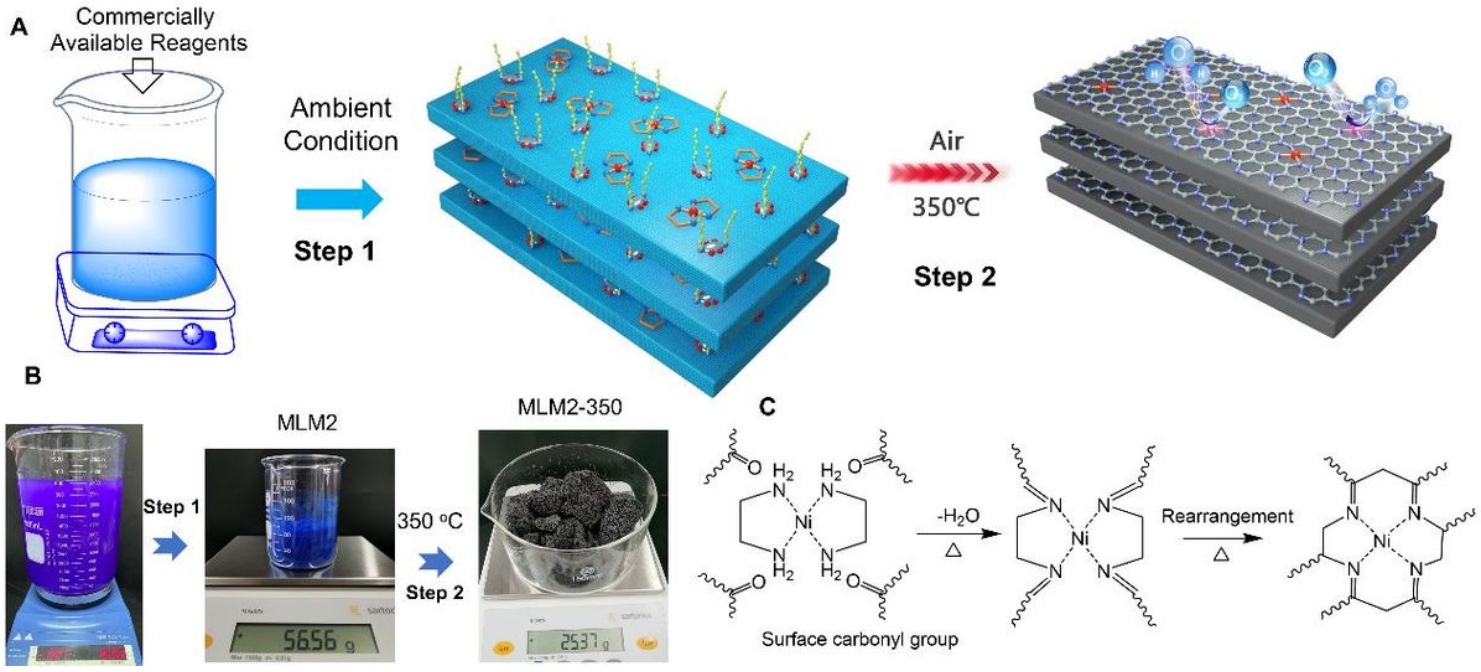

Figure 1

Schematic diagram for the preparation of NiN_x-SAC MLM2-350. **A**. The two steps synthesis of MLM2-350; Step 1, Emulsion synthesis of NiN_x precursor doped layered Co coordination polymer; Step 2, Surface immobilization of NiN_x site under thermal treatment. **B.** Tens-grams scale preparation of MLM2 and MLM2-350 from one batch. **C**. Proposed reaction mechanism for the immobilization of NiN_x sites on the surface.

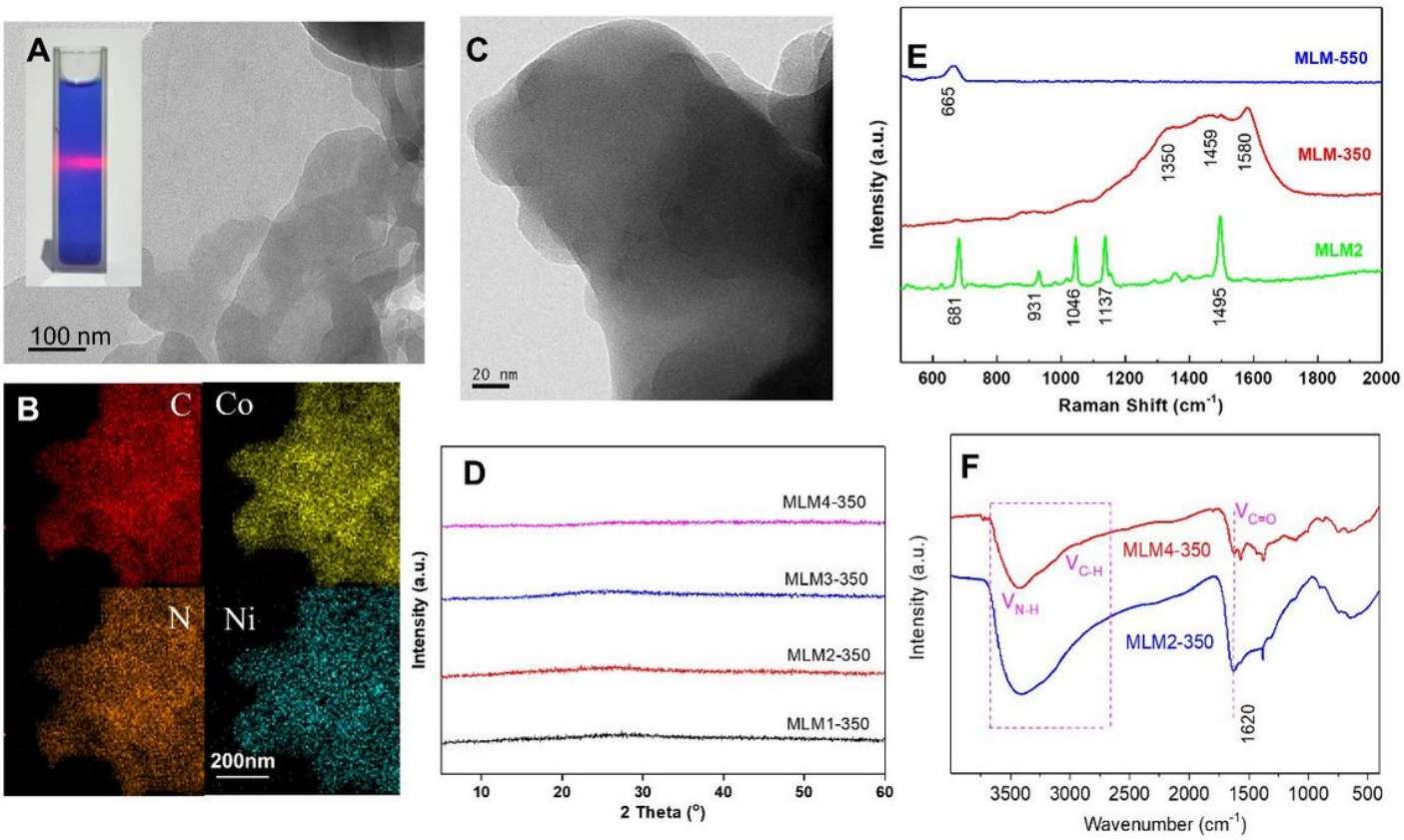

Figure 2

Characterizations of the MLM samples. **A.** TEM image of MLM nanosheet, inset, Tyndall effect of the MLM nanosheet suspension; **B.** Element maps of MLM2 showing distributions of C (purple), Ni (cyan), Co (green), and N (yellow); **C.** TEM image of MLM2; **D**. Powder XRD of different MLM-350 samples; **E**. Raman spectra of MLM2(green), MLM2-350(red) and MLM2-550 (blue); **F**. Comparation of IR spectra for MLM2-350 and MLM4-350.

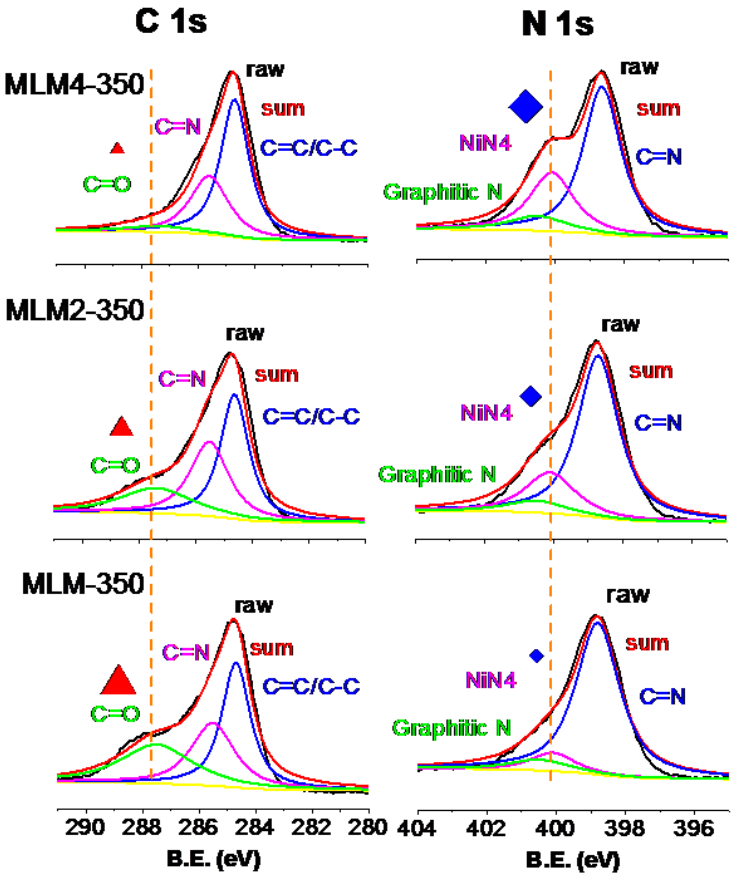

Figure 3

Comparation of C 1s and N 1s XPS spectra for MLM-350, MLM2-350, MLM4-350.

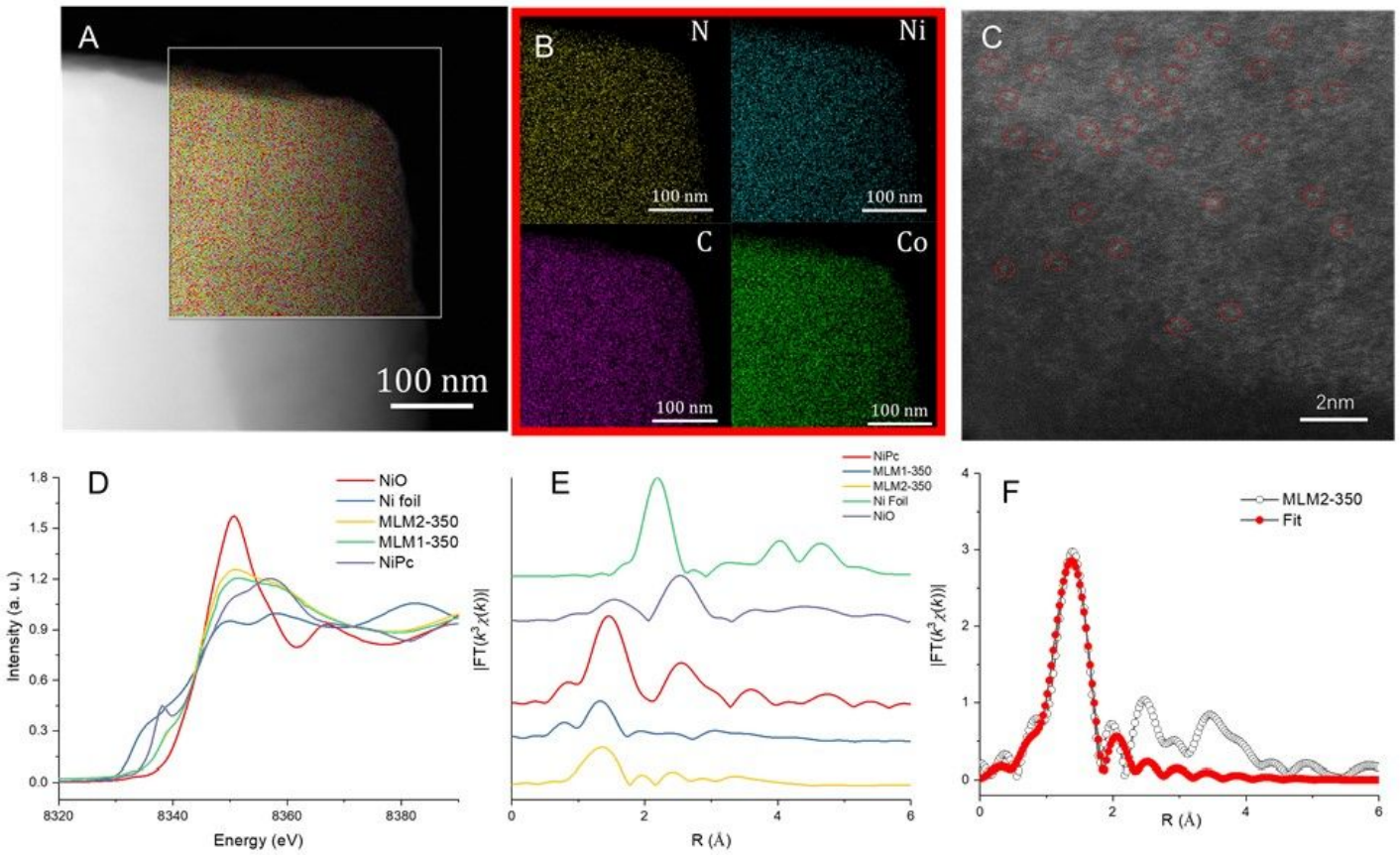

Figure 4

Structural characterization of NiN_x sites immobilized on the layer surface. **A**, HAADF-STEM image and overlapped element mapping image of MLM2-350; **B**, Element mapping showing distributions of C (purple), Ni (cyan), Co (green), and N (yellow); **C**, Aberration-corrected HAADF-STEM image of MLM2-350; **D**, Normalized Ni K-edge X-ray absorption near-edge structure XANES spectra of MLM samples with reference samples; **E**, Fourier transformed magnitudes of the experimental Ni K-edge EXAFS signals of MLM samples with reference samples. **F**, EXAFS fitting curve for MLM2-350.

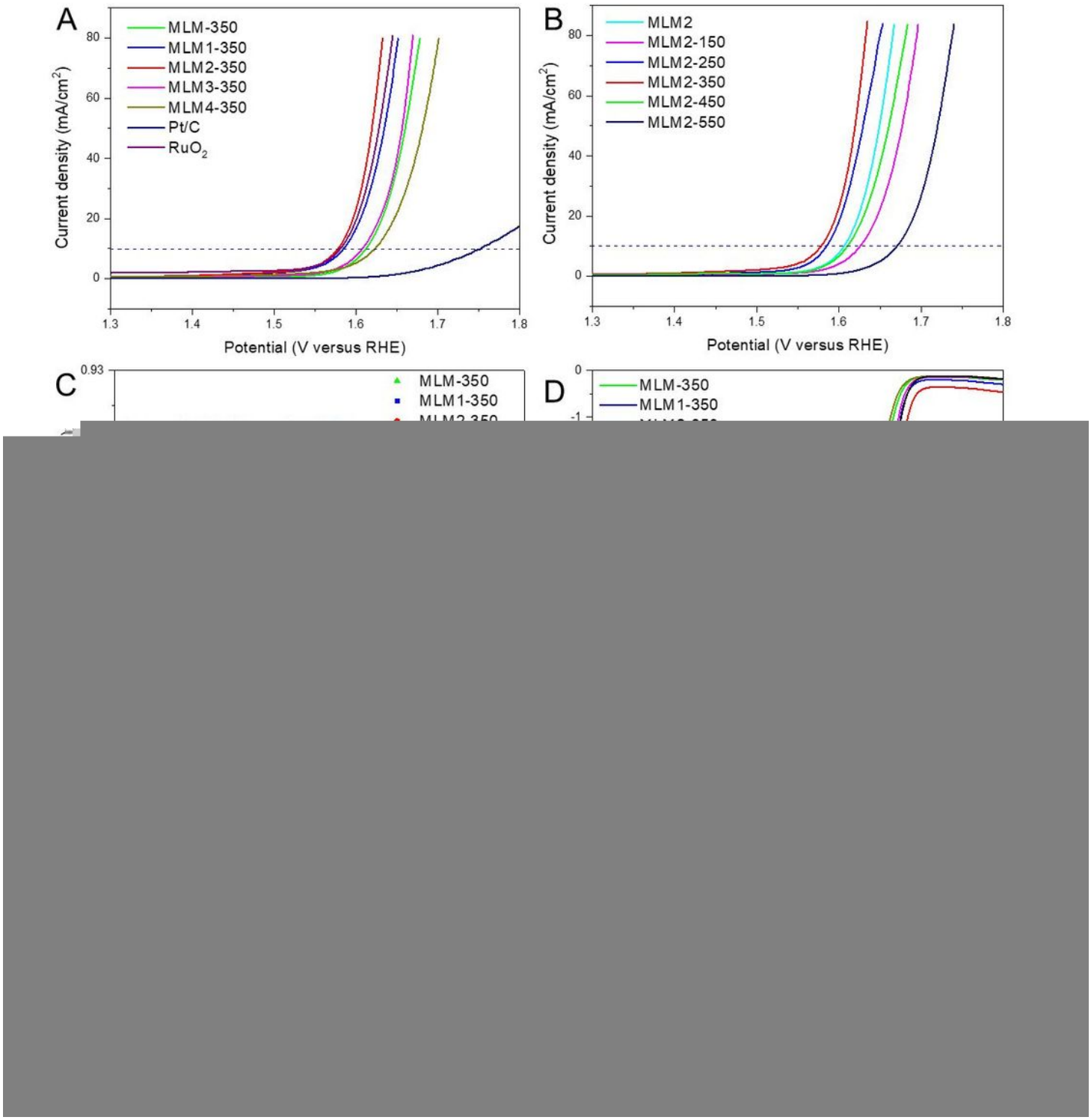

Figure 5

The electro-catalysis performance of MLM samples. OER polarization curves of (A) MLM samples pyrolyzed under 350 ^{o}C with different Co/Ni ratio and (B) MLM2 samples pyrolyzed under different temperatures. (C) Tafel slopes of MLM-350 samples in OER. OOR polarization curves of (D) MLM samples pyrolyzed at 350 ^{o}C with different Co/Ni ratio (sweep rate = 5 mV/s and 1600 rpm). (E) Overall

polarization curves MLM2-350 samples and the bifunctional ORR/OER activities (ΔE). All tests were performed in 1.0 M KOH solution.

Supplementary Files

This is a list of supplementary files associated with this preprint. Click to download.

- SupportInformation.pdf